Molecular quantum interface for storing and manipulating ultrashort optical vortex

Firas Trawi, Franck Billard, Olivier Faucher, P. Béjot, Edouard Hertz

Abstract Light beams carrying orbital angular momentum (OAM) have become over the past few years a subject of widespread interest with unprecedented applications in various fields such as optical communication, super-resolution imaging, optical tweezers, or quantum processing. We demonstrate in the present work that gas-phase molecules can be used as a quantum interface to store an OAM carried by an ultrashort laser pulse. The interplay between spin angular momentum and OAM is exploited to encode the spatial phase information of light beams into rotational coherences of molecules. The embedded spatial structure is restored on-demand with a reading beam by taking advantage of field-free molecular alignment. The strategy is successfully demonstrated in CO_2 molecules at room temperature. Apart from applications to broadband coherent buffer memory, the method opens new functionalities in terms of optical processing and versatile control of OAM fields as well as for a deeper understanding of their role on various molecular processes.

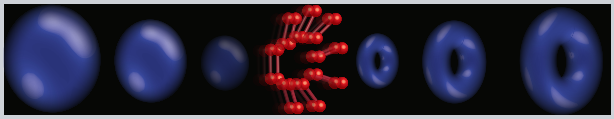

GUIDE

Molecular quantum interface for storing and manipulating ultrashort optical vortex

Firas Trawi, Franck Billard, Olivier Faucher, Pierre Béjot and Edouard Hertz*

1. Introduction

Angular momentum is one of the most fundamental physical properties of photons. Besides the spin angular momentum (SAM) associated with the polarization state, light beams can also carry an orbital angular momentum (OAM) related to the wavefront shape. While OAM beams have long been considered as a marginal effect mainly related to multipolar transitions, Allen *et al.* established in 1992 that beams of transverse phase distributions $e^{i\ell\varphi}$ (with φ the azimuthal coordinate in the cross section of the beam) carry an orbital angular momentum of $\ell\hbar$ per photon. [1] The ℓ-value, corresponding to the phase winding number, is called topological charge and can take any positive or negative integer values. Due to their unique properties, [2,3] helically phased beams or vortex beams have triggered a broad range of research covering optical communication, [4–7] transfer of OAM to microscopic particles in optical tweezers, [8,9] rotational Doppler effect, [10] nonlinear interaction [11] and high harmonic generation, [12–14] modification of selection rules in atomic transitions due to this additional angular momentum [15] or chirality and optical activity [16] to name a few. While the spin angular momentum of light has only two orthogonal states, the OAM has in principle an unlimited number of eigenstates being of significant interest for quantum technologies [17,18] and data storage of high capacity. A large number of studies has therefore focused on the development of quantum memories for OAM, [19–21] storing the phase information into internal states of atoms (usually between two ground states via a resonant three-level excitation). Here we show that the OAM of an ultrashort pulse can be encoded into a superposition of molecular rotational states and readout later on by exploiting the mechanism of laser-induced field-free molecular alignment. This regime of alignment received increasing attention in the past twenty years. [22–25] It is well-known that molecules exposed to a non-resonant and intense laser pulse can be aligned by the electric field as a result of the anisotropic interaction with the induced dipole. In the case of a short pulse (of duration much shorter than the rotational period), the interaction prepares a broad rotational wavepacket in the vibronic ground state of the molecule by impulsive stimulated Raman transitions. After the pulse turn-off, the quantum beatings of the wavepacket lead to molecular alignment at well defined times under field-free conditions. [26,27] Such a regime of laser-induced molecular alignment has been extensively applied in various fields of physics extending to ionization, [28] harmonic generation and attophysics, [29] rotational Doppler effect, [30,31] collisional dissipation, [32] laser filamentation, [33,34] or in the context of ultrafast imaging technology for optical image storing. [35,36] We show here its potentiality for storing the phase front of an ultrashort light embedding an OAM analogously to holographic imaging. The demonstration is conducted with CO_2 molecules at room temperature. The choice of CO_2 was mo-

Laboratoire Interdisciplinaire Carnot de Bourgogne, UMR 6303 CNRS - Université Bourgogne Franche-Comté, 21078 Dijon Cedex, France
* Corresponding author: e-mail: edouard.hertz@u-bourgogne.fr

tivated by its high value of polarizability anisotropy but the method is applicable to all molecules except spherical top molecules. The molecular alignment is probed by polarization technique. [27,37] The non-resonant excitation scheme exploits the interplay between SAM and OAM so as to produce a rotational wavepacket in the vibronic ground state of CO_2 that memorizes the OAM information, this last being restored by the periodical rephasing of the wavepacket leading to field-free molecular alignment. Unlike most previous works, the method provides a coherent buffer memory of OAM carried by femtosecond pulses. We demonstrate the possibility to encode and read out OAM modes with a great fidelity. Besides ultrafast quantum processing, the use of rotational states as a quantum interface could open new attributes and modalities in view of the strong impact of molecular alignment on a wide range of processes. Furthermore, the different well established strategies enabling a versatile control of molecular alignment or unidirectional rotation, such as pulse shaping [38,39] or polarization shaping, [30,31] could also be very valuable for the manipulation of ultrashort optical vortex.

2. Method

2.1. Coupling scheme

In the present experiment, the spin angular momentum and orbital angular momentum are conserved on their own. The weak focusing geometry of the driving field prevents any spin-to-orbital conversion occurring in high numerical aperture lens focusing. [40] Furthermore, since dipole electric transitions are allowed, quadrupole transitions will weakly contribute to the overall signal so that standard selection rules of dipole electric transition can apply without any modifications accounting for OAM. [15] As a result, any combination of spin (or orbital) angular momenta conserving the initial spin (or orbital) angular momentum of light is allowed, namely $\Delta\ell = \sum \ell^{abs} - \sum \ell^{emit} = 0$ for the OAM and $\Delta s = \sum s^{abs} - \sum s^{emit} = 0$ for the SAM (where *abs* and *emit* denote the absorbed and emitted photons respectively). We emphasize that the SAM carried by the light acts on the magnetic quantum number M of molecular states while the OAM does not modify the internal states. This set of rules is used to identify the suitable excitation scheme enabling the storage of light's OAM into molecular rotational states. For encoding OAM modes or complex images into internal states of atoms, excitation schemes are usually based on a resonant Λ-configuration using Stokes and anti-Stokes beams of different helical phase fronts. In most cases, a Stokes beam of topologic charge ℓ together with an anti-Stokes $\ell = 0$ beam (called "Gaussian beam" hereafter) are used. With such a configuration, the phase difference $\ell\varphi$ between the beams is stored through the coherences induced between the two ground states and retrieved at will with a reading beam. Direct application of such a strategy in the context of molecular alignment turns out to be ill-suited because the rotational coherences are produced between a great number of states belonging to the same vibronic state using a short and broadband pulse. The Stokes and anti-Stokes field of same central frequency cannot therefore be distinguished leading to unwanted quantum excitation channels. These lasts can be avoided using circularly polarized (CP) fields by means of the spin selection rule. Let's consider a pump field producing the molecular alignment written as:

$$\vec{E}(t) = \varepsilon_0(t)e^{-i\omega_0 t}\left(\hat{\sigma}_- + e^{i\ell\varphi}\hat{\sigma}_+\right), \qquad (1)$$

where $\hat{\sigma}_+$ ($\hat{\sigma}_-$) corresponds to the right (left)-handed circular polarization in the (x,y) plane $\hat{\sigma}_\pm = \frac{1}{\sqrt{2}}(1, \mp i)$, called RCP (LCP) hereafter. When interacting with the molecular sample, this pump field induces rotational coherences and field-free molecular alignment. If a time-delayed LCP probe pulse reads the molecular medium at the occurrence of transient alignment, a field of opposite helicity is produced due to the sample anisotropy. This last, called signal field, can be isolated by a circular analyzer and is expected to carry the same topological charge as the one embedded in the $\hat{\sigma}_+$ pump component owing to SAM and OAM conservation. This point is illustrated in Figure 1. As it can be seen, the $\hat{\sigma}_-$ probe and $\hat{\sigma}_+$ signal field imply $\Delta J = 0, \pm 2$ and $\Delta M = -2$ transitions, where J and M correspond to the total angular momentum and magnetic quantum numbers, respectively (with the quantum axis chosen along the propagation axis $\vec{e}_z$). The SAM conservation therefore imposes the sequence of pump pulses helicity in the overall parametric cascaded process and consequently the topological charge ℓ of the signal field by OAM conservation. We point out that the use of linear polarizations would lead to three additional excitation channels: two channels storing $\ell = 0$ and corresponding to an excitation only driven by the OAM beam or the Gaussian beam and another channel storing -ℓ corresponding to the exchange between the Stokes and anti-Stokes fields for the pump [see Section 3, Supporting information]. The SAM conservation and spin constraint therefore enables to get rid of this unwanted superposition. Such an interplay between spin and orbital angular momentum has been exploited to

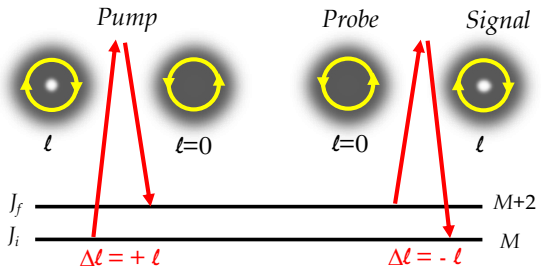

Figure 1 Coupling scheme for encoding the phase information of OAM beams into rotational states of molecules by SAM and OAM conservation, the allowed transitions are $\Delta J = J_f - J_i = 0, \pm 2$, $\Delta M = -2$ ($\Delta M = +2$) for the probe (pump) interaction. $\Delta\ell = +\ell$ for the first step corresponds to the ℓ-value stored by the molecular sample and restored later on into the signal field via the reading process.

control the OAM states of harmonic fields produced by up-conversion process. [14]

2.2. Theoretical model

In order to go further in the analysis and confirm the previous qualitative approach, we write the time-dependent Hamiltonian describing the coupling of the molecule to a non-resonant external field as introduced in Eq. 1, namely with polarization components in the circular basis written as:

$$E_+(t,\varphi) = \varepsilon_0(t)e^{-i(\omega_0 t-\ell\varphi)} \quad (2)$$

$$E_-(t) = \varepsilon_0(t)e^{-i\omega_0 t}. \quad (3)$$

Within the high-frequency approximation, one can show [see Section 1, Supporting information] that this Hamiltonian writes as:

$$H(t) = BJ^2 - DJ^4 - \frac{\varepsilon_0(t)^2}{2}\left[\alpha_\perp + \Delta\alpha\sin^2\theta\cos^2\left(\Phi - \frac{\ell\varphi}{2}\right)\right], \quad (4)$$

where the first term corresponds to the field-free Hamiltonian with B the rotational constant, D the centrifugal distortion constant [B=0.39 cm^{-1} and D=1.33 10^{-7} cm^{-1} for CO_2], and J^2 the angular momentum operator. The second term of Eq. 4 corresponds to the interaction Hamiltonian where $\Delta\alpha = \alpha_\parallel - \alpha_\perp$ is the difference between the parallel and perpendicular components of the polarizability tensor, while θ and Φ are the polar and azimuthal angles of the molecule (θ is the angle between the molecular axis and the laboratory $\vec{z}$-axis, and Φ is the angle of rotation of the molecule around $\vec{z}$).

The interaction Hamiltonian indicates that the molecules will preferentially be confined in the (x,y) plane (i.e. with $\theta = \pi/2$) while being aligned along the direction defined by the polar angle $\Phi = \frac{\ell\varphi}{2}$ (with respect to the laboratory $\vec{x}$-axis). The molecular axis orientation therefore depends on the azimuthal angle φ in the beam's section so that a probe beam $E_{\rm pr}(t)$ interacting with such an inhomogeneous medium will experience a spatially-dependent modification of its ellipticity which is at the origin of the OAM carried by the signal field. This last can be inferred from the expression of the dipole moment induced by the LCP probe field $\vec{\mu}_{\rm pr} = \frac{1}{2}\vec{\vec{\alpha}}E_{\rm pr}(t)\hat{\sigma}_-$. After the circular analyzer selecting the field of opposite handedness, the signal field [see Section 2, Supporting information] writes as:

$$E_{\rm sig}(t,\varphi) \propto \left\langle \hat{\sigma}_+^{\rm T}\vec{\mu}_{\rm pr}\right\rangle \propto \Delta\alpha\left\langle \sin^2\theta e^{i2\Phi}\right\rangle E_{\rm pr}(t), \quad (5)$$

where $\langle..\rangle$ denotes the quantum averaged value. For a probe pulse time-delayed by τ of the form $E_{\rm pr}(t) = \varepsilon_0(t-\tau)e^{-i\omega_0(t-\tau)}$ and a molecular alignment along $\theta \approx \pi/2$ and $\Phi \approx \frac{\ell\varphi}{2}$, the signal field becomes:

$$E_{\rm sig}(t,\varphi,\tau) \propto \Delta\alpha\varepsilon_0(t-\tau)e^{-i(\omega_0(t-\tau)-\ell\varphi)} \propto E_+(t-\tau,\varphi) \quad (6)$$

which is a copy of the (pump) Stokes field encoded in the molecular sample. As a result, any topological charge ℓ can in principle be memorized by the molecules as expected by SAM and OAM conservation through the diagram of Figure 1.

3. Experimental set-up

The experimental set-up is depicted in Figure 2. The laser system delivers pulses of 35 fs duration centered around 800 nm at 1 KHz repetition rate and with a maximum energy of 6 mJ. The input beam is split in two parts by a 80/20 beam splitter so as to produce the pump and probe beams. The probe beam is frequency doubled with a BBO-crystal (the remaining fundamental frequency being rejected from the probe beam path with a polarizer). The use of a probe field with a central frequency different from that of the pump allows to reject the pump field after the interaction. The probe is then circularly polarized using a Berek compensator (BC_1). The pump passes through a motorized delay line and a beam shaper for imprinting its spatial structuring. Pump and probe beams are colinearly recombined by an optical wedge before being focused by a lens L_1 (f=30 cm) in a static gas cell filled with 0.7 bar of CO_2. At the exit of the cell, the beams are collimated by a lens L_2 (f=25 cm) and a circular analyzer (consisting of a Berek compensator BC_2 and polarizer) analyzes the signal field of interest corresponding to the depolarization of the probe beam. The signal field, isolated from the pump using a dichroïc filter (F), can be measured either by a CCD camera (providing a signal $S(\varphi,\tau) \propto \int \left|E_{\rm sig}(t,\varphi,\tau)\right|^2 dt$) or by a photomultiplier tube (PMT) giving the spatially-integrated signal. The spatial phase profile and OAM state is obtained by measuring the interference pattern with a reference Gaussian beam of same polarization state. We emphasize that the use of Berek compensators instead of quarter waveplates for the probe beam is motivated by the possibility of inducing a tunable phase shift which can be adjusted as a function of the wavelength and by the possibility of precompensating the birefringence induced by optical reflections.

The spatial structuring of the pump beam is realized by means of a q-plate that is used for generating OAM beams via SAM-OAM exchange occurring in both anisotropic and inhomogeneous media. A q-plate is a birefringent material whose slow (or fast) axis orientation varies continuously with the azimuthal angle φ according to the pattern defined by [41]

$$\alpha(\varphi) = q\varphi, \quad (7)$$

where α denotes the angle between the neutral axis and the x-coordinate axis, and q the topological charge of the plate which can be integer or half-integer. The OAM number generated by a q-plate is $\ell = \pm 2q$ and the transformation experienced by a $\hat{\sigma}_\pm$ beam propagating through a q-plate

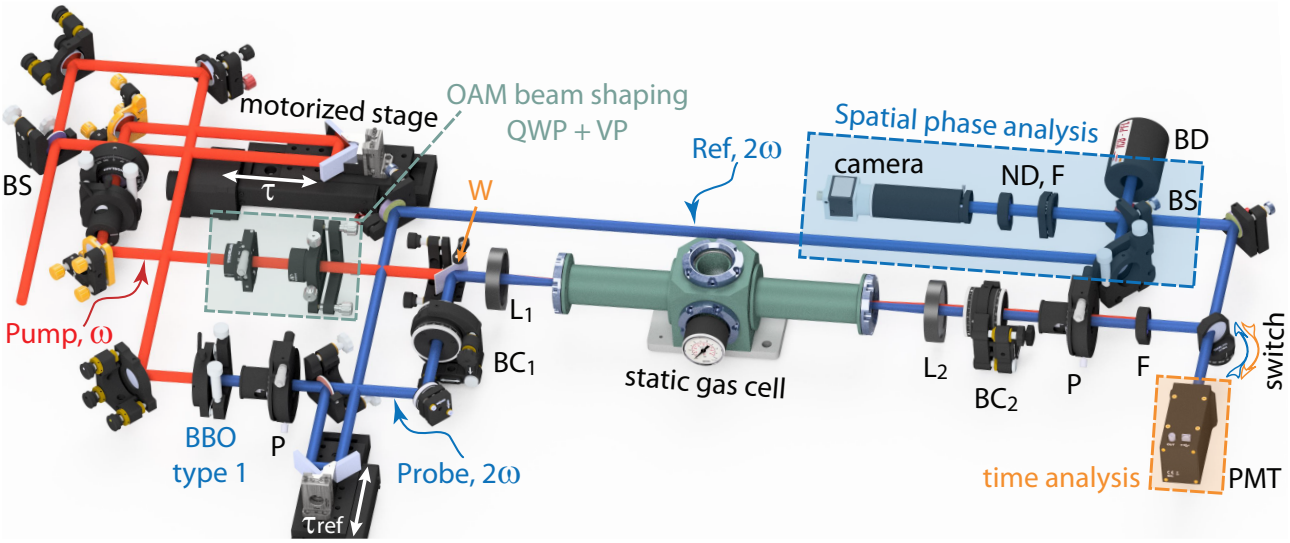

Figure 2 Experimental set-up. BS: beam splitter, QWP: quarter waveplate, VP: vortex plate [$\delta = \pi/2$, $q = 1/2$], W: wedge, BBO: type 1 doubling crystal, P: Polarizer, L: plano-convex lens, BC: Berek compensator, PMT: photomultiplier tube, BD: beam dump, F : 400 nm bandpass filter, ND: neutral density filter.

can be described [41,42] using a unitary operator $\hat{U}$:

$$\hat{U}\hat{\sigma}_- = \cos\left(\frac{\delta}{2}\right)\hat{\sigma}_- \pm i\sin\left(\frac{\delta}{2}\right)e^{+2iq\varphi}\hat{\sigma}_+ \qquad (8)$$

$$\hat{U}\hat{\sigma}_+ = \cos\left(\frac{\delta}{2}\right)\hat{\sigma}_+ \pm i\sin\left(\frac{\delta}{2}\right)e^{-2iq\varphi}\hat{\sigma}_-, \qquad (9)$$

where δ denotes the phase retardation of the plate. The sign $\pm$ between the two components depends on whether the angle α in Eq. 7 relates to the slow or the fast axis: + (resp. -) for slow (resp. fast) axis.

The first conducted experiment aimed to store a pure ($\ell = 1$) OAM in the molecular sample. In this purpose, a beam shaper consisting of a quarter waveplate and a q-plate has been used. The q-plate was designed with a phase retardation $\delta = \pi/2$ (quarter waveplate) and an azimuthal distribution of its fast axis as in Eq. 7 with $q = 1/2$. According to Eq. 8, such a q-plate converts a beam $\hat{\sigma}_-(\ell = 0) \rightarrow 1/\sqrt{2}\,[\hat{\sigma}_-(\ell = 0)\text{-i }\hat{\sigma}_+(\ell = 1)]$ which is exactly the overall Stokes and anti-Stokes pump depicted in Figure 1. This q-plate therefore enables to produce the global excitation field at once. We emphasize that the relative phase of $-\pi/2$ between the two components is not important for our purpose since it only gives rise to an angular rotation of the OAM field.

4. Results

The alignment signal was first recorded as a function of the pump-probe delay for a pump energy of 15 μJ, the pump beam being composed of two different topological charges with different helicities [$\hat{\sigma}_-(\ell$=0), $\hat{\sigma}_+(\ell$=1)]. Such an energy corresponds to a weak field excitation regime of the molecular sample. Typical pump-probe signal measured by the PM using this configuration is depicted in blue line of Figure 3. This last reflects a standard field-free alignment trace of CO_2 [27,43] with transient alignment revival located every $T_r/4$=10.68 ps, with $T_r = \frac{1}{2Bc}$ the rotational period. The structural shape of the revivals is governed by the conditions of rephasing of the rotational wavepacket [see Section 5, Supporting information]. The signal gradually decreases because of the molecular wavepacket decoherence induced by collisional relaxation so that in the present experimental conditions with a pressure of 0.7 bar, the alignment vanishes after approximately 100 ps. [44] It should be pointed out that the storage time can reach several nanoseconds [45] if the gas density is reduced. The intensity pattern of the beam has been measured with the camera for different delays. The result, depicted in insets in Figure 3, displays the typical signature of helically phased beams with the well-known doughnut shape resulting from the phase singularity on the beam axis. This annular intensity pattern is a strong indication that molecules have stored the OAM state (ℓ=1) carried by the Stokes pump field before restoring it when interacting with the delayed probe pulse. In order to verify this claim, the interference pattern with a synchronized reference beam crossing at small angle (0.5°) has been measured. The recorded measurement is displayed in Figure 4b for the delay $\tau = 21.18$ ps (labeled ① in Figure 3). This interferogram exhibits the usual fork-shaped pattern providing after spatial Fourier filtering, the spatial phase of the signal beam. The reconstructed spatial phase, depicted in Figure 4c, is shown to wrap counter-clockwise from 0 to 2π, which confirms the helical phase structure of topological charge $\ell = 1$ of the signal field. It can be noticed a residual spiral-like pattern in the retrieved phase which can be explained by a slight difference of curvatures of the OAM and reference beams. The underlying mechanism of the present result can

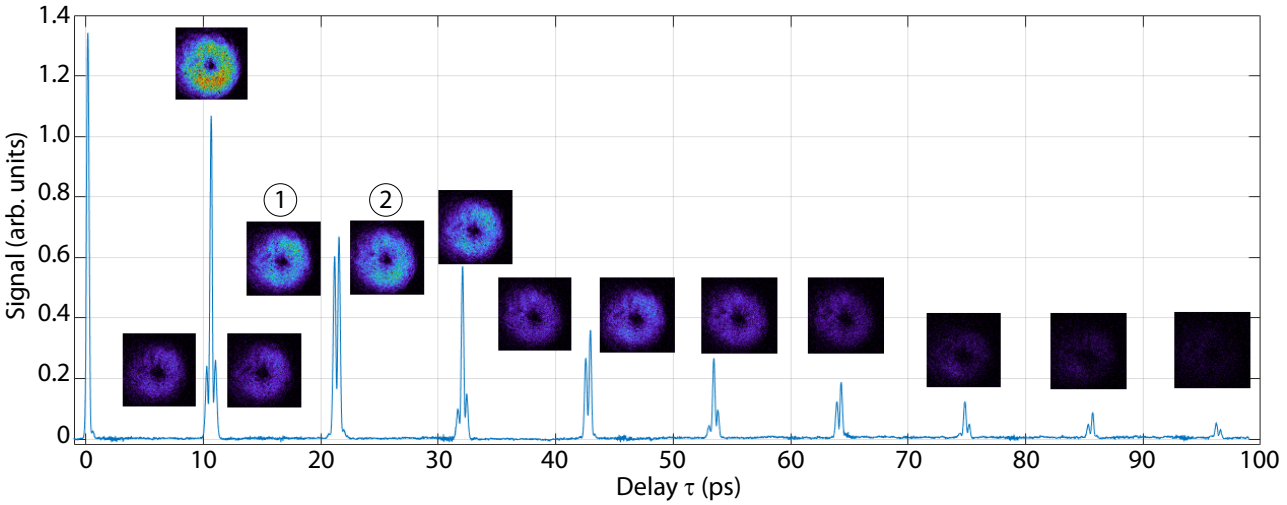

Figure 3 Alignment signal of CO_2 (blue solid line) as a function of the pump-probe delay for a pump energy of 15 μJ recorded with the photomultiplier tube. The insets correspond to the intensity pattern of the signal recorded by the camera around delays corresponding to revivals of alignment.

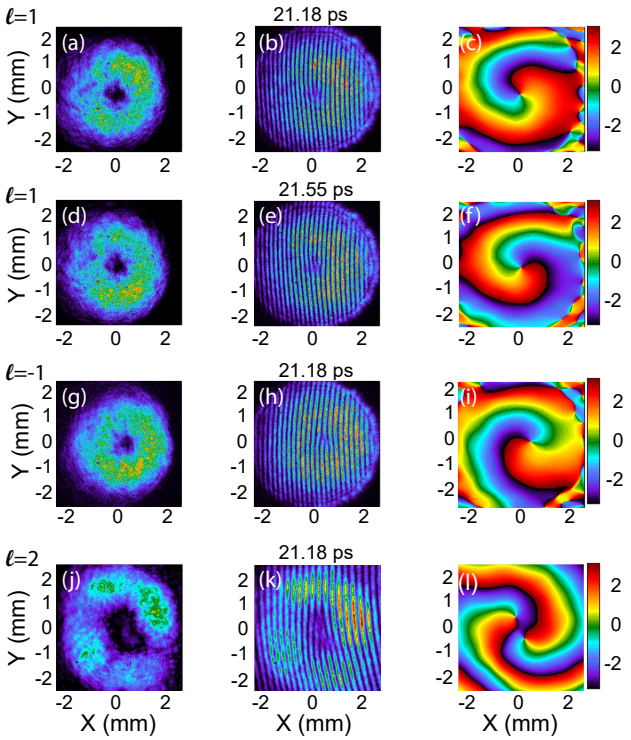

Figure 4 First line: (a) intensity pattern of the signal recorded by the camera, (b) interferometric intensity pattern, and (c) retrieved spatial phase for $\ell = 1$ and $\tau = 21.18$ ps corresponding to a peak of alignment. Second line: same as first line but for $\tau = 21.55$ ps corresponding to a peak of planar delocalization. Third line: same as first line but for the storage of $\ell = -1$. Fourth line: same as first line but for the storage of $\ell = 2$.

be interpreted as the production of a "molecular q-plate". According to Eqs. 8-9, in order to produce a beam carrying an OAM quantum number $\ell = 1$, one should use a q-plate with $q = 1/2$ namely with neutral axis orientation defined by $\alpha(\varphi) = \frac{\varphi}{2}$. A quick inspection of Eq. 2-3 reveals that the combination of the two pump components $\hat{\sigma}_-(\ell = 0)$ and $\hat{\sigma}_+(\ell = 1)$ writes in the $(\vec{e}_x, \vec{e}_y)$ basis as:

$$\vec{E}(t) = \sqrt{2}\varepsilon_0(t)e^{-i(\omega_0 t - \frac{\varphi}{2})}\left[\cos(\frac{\varphi}{2})\vec{e}_x + \sin(\frac{\varphi}{2})\vec{e}_y\right], \quad (10)$$

producing a polarization vector distribution that exactly follows the pattern $\alpha(\varphi) = \frac{\varphi}{2}$ of a q-plate ($q = 1/2$). The molecular alignment induced by such a field will therefore follow the same azimuthal pattern, i.e. $\Phi(\varphi) = \alpha(\varphi)$ resulting in the formation of a "molecular q-plate". This point is illustrated in Figure 5a depicting the polarization pattern of the pump beam together with the spatial distribution of alignment induced by this last. The modification of a LCP probe beam interacting with the molecular sample (Figure 5b) can be inferred from Eq. 8 using $q = 1/2$, δ that depends on the degree of alignment $\langle \sin^2\theta e^{i2\Phi} \rangle$ in Eq. 5, and a + sign between the two components due to the orientation of the molecular slow axis. As a result, when the LCP probe field propagates through the medium, the output field consists of a combination of $\hat{\sigma}_-(\ell = 0)$ and $\hat{\sigma}_+(\ell$=1) beams, in perfect agreement with the expectation of Figure 1. The circular analysis enables the selection of the last component carrying the OAM mode. The SAM-OAM conversion experienced by the probe beam is allowed by the inhomogeneous anisotropy of the molecular sample associated to the spatial distribution of molecular alignment.

It is well-known that the rephasing of the rotational wavepacket around $\tau = 21.18$ ps correspond to a situation where the molecules realign along the direction of the pump polarization axis so that the configuration matches the one of Figure 5b. Nevertheless, the time-dependent dynamics of molecular alignment is more complex and also contains "planar delocalization" peaks [see Section 5, Supporting in-

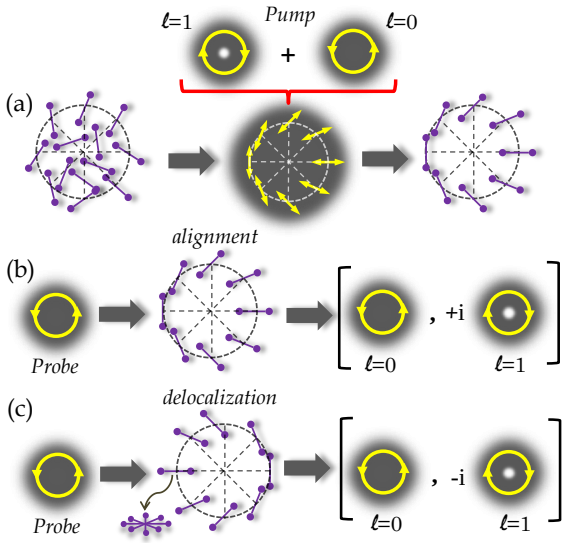

Figure 5 (a) Illustration of the $\ell = 1$ OAM storage mechanism: the superposition of ($\hat{\sigma}_+$, $\ell = 1$) and ($\hat{\sigma}_-$, $\ell = 0$) pump fields provides an azimuthal distribution of polarization inducing a molecular alignment with the same pattern (equivalent to a q-plate with $q = 1/2$ see text). (b) A LCP probe field interacting with this molecular sample at the occurrence of molecular alignment produces a field of opposite handedness carrying an OAM of topological charge $\ell = 1$. (c) same as (b) but for a delay corresponding to a planar delocalization.

formation] during which the molecules are preferentially located in a plane perpendicular to the pump polarization axis. [26,27] It is interesting to analyze the effect of such a molecular distribution on the restored OAM. Figures 4(d-f) show the same measurements as in Figs. 4(a-c) but for the adjacent peak of the same revival at $\tau = 21.55$ ps (labeled ② in Figure 3) and corresponding to an occurrence of planar delocalization. As it can be seen, the phase retrieved from the interference pattern still exhibits a counter-clockwise winding characteristic of a topological charge $\ell = 1$. This observation indicates that any delay can be used to read out the encoded information. The main difference between the two configurations (measured in the same conditions) lies in a global rotation of 180° of the spatial phase. This observation can be understood by considering that for a planar delocalization (Figure 5c) the molecular orientation in the (x,y) plane follows the distribution $\Phi \approx \frac{\varphi}{2} \pm \frac{\pi}{2}$ (instead of $\Phi \approx \frac{\varphi}{2}$ for a molecular alignment) leading to a signal field (Eq. 5) carrying a phase $\varphi \pm \pi$ and therefore a helical phase front ($\ell = 1$) with a π-angular shift. Note the very short switching time between the two configurations. This property could be exploited (see discussion) to produce an ultrashort pulse carrying a helical phase structure that rotates within the pulse envelope. As a further demonstration of the method, we have also stored an OAM of opposite chirality $\ell = -1$. Following Eq. 9, a RCP field has been injected into our q-plate [q=1/2, $\delta = \pi/2$] leading to the transformation $\hat{\sigma}_+(\ell = 0) \rightarrow 1/\sqrt{2}$ [$\hat{\sigma}_+(\ell = 0)$-i $\hat{\sigma}_-(\ell = -1)$]. Since the pump components carrying $\ell = -1$ and $\ell = 0$ are reversed compared to the previous case, the probe helicity and circular analysis have also been reversed. The coupling scheme is then the one of Figure 1 but with $\ell = -1$ and circular polarization of opposite handedness for all fields. The retrieved phase for the alignment peak ($\tau = 21.18$ ps) shown in Figs. 4(g-i) turns out to exhibit the clockwise winding distribution characteristic of a ($\ell = -1$) OAM state. Finally, as a proof of generality, an OAM state of topological charge $\ell = 2$ has been stored into the molecular sample. The reconstructed phase of the signal field, depicted in Fig. 4(l), exhibits a continuous counter-clockwise increase from 0 to 4π with two spiral arms as expected for a beam carrying a $\ell = 2$ OAM number. Another noticeable feature in the doughnut shape intensity pattern of Fig. 4(j) is the larger dark core compared to the previous cases $\ell = \pm 1$. This is a further signature of an increase in ℓ value, the radial nodes evolving as $r^{|\ell|}$. This last example confirms the ability of the method to store any OAM state as predicted by the theoretical model (section 2.2).

The present result demonstrates the potential of using molecular systems as a quantum interface to store an OAM embedded in ultrashort light. Such a coherent buffer memory is attractive for ultrafast local quantum processing where long storage times are not required. While the storage time is a crucial parameter for long-distance communication, other properties as the bandwidth and multi-mode capacity may be of more interest when local quantum processing applications are concerned. [46] The upper method demonstrating the storage of THz-bandwidth light falls into this category. Additionally, the non-resonant Raman memory of the present coupling scheme allows to re-encode the stored helical phase-front structure to any beams of different wavelength. However, one could emphasize one limitation. When exposed to a moderately intense pump beam, the molecules align periodically during the revivals but the effect remains weak in between so that the signal is hardly readable. We point out that the readout sampling rate depends on the moment of inertia of the molecule and can therefore be controlled by changing the molecular system. Nevertheless, the readout cannot be considered truly on-demand. A similar limitation is known for other quantum memory protocols with multi-mode ability as controlled-reversible inhomogeneous-broadening (CRIB [47]) or atomic frequency comb (AFC [48]), which rely on the control of an inhomogeneously broadened optical transition. In CRIB, the atomic polarization has to rephase after the broadening has been reversed, while in AFC the rephasing time is fixed by the comb spacing. In our case, this limitation can be however circumvented by the use of a stronger pump field interaction that manifests itself by the occurrence of a residual alignment between the revivals [see Section 5, Supporting information] called "permanent" alignment. [22,26,27] This steady-state alignment lets envision to consider an on-demand readout of the OAM state. So as to check this property, the same experiment has been repeated with a pump energy of 160 μJ. The result displayed in Figure 6 shows, in addition to the signal obtained during the alignment revivals, a background signal which is the manifestation of the permanent alignment process. Recording the intensity pattern of the signal

between two alignment revivals (here at τ =5 ps) indeed reveals that the OAM state embedded within the pump can be restored at any time (up to the coherence time of the memory) confirming the potential of permanent alignment for a truly on-demand readout. An additional advantage of the permanent alignment lies in its robustness against collisional relaxation. Indeed, it has been shown [49] that collisions induce a decay of the permanent alignment about twice slower than that of the transient revivals amplitudes.

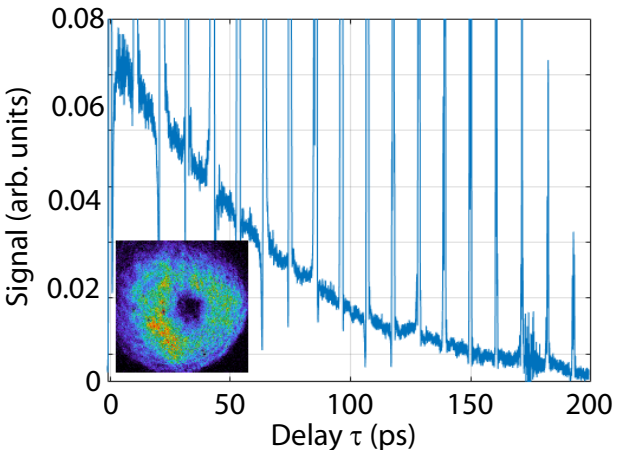

Figure 6 Alignment signal of CO_2 (blue solid line) as a function of the pump-probe delay for a pump energy of 160 μJ recorded with the photomultiplier tube. A zoom on the signal is applied to better visualize the permanent alignment and the signal decay is due to collisional relaxation. The image corresponds to the intensity pattern of the signal recorded at 5 ps between two revivals.

5. Conclusion and discussion

We have successfully demonstrated the storage of helical phase structures carried by ultrashort pulses into the rotational coherences of a molecular system. The demonstration is conducted in CO_2 molecules at room temperature in which $\ell = \pm 1$ or ℓ=2 OAM states have been stored and readout on demand with a reading beam. We emphasize that the method is not limited to the use of CO_2 molecules as a quantum interface, similar results to those presented in this work have been obtained with N_2. The underlying mechanism relies on the production of a gas-phase molecular q-plate resulting from the occurrence of laser-induced field-free molecular alignment. This experimental work constitutes a first step and provides the guidelines before a forthcoming experiment aiming at storing a coherent superposition of OAM states (i.e. qubits) into rotational wavepackets. The present approach is indeed well-suited for encoding both spatial phase and amplitude information of structured light beams. The broad distribution of molecular rotational states could also be exploited to achieve unprecedented storage capability. A real breakthrough in the manipulation of beam light has been recently achieved with the production of space-time wavepackets embedding time-varying OAM characteristics. [50] To reach this goal, different OAM states have been encoded into distinct spectral bands of the laser spectrum (in addition to an overall temporal shaping applied in the frequency domain). The present method could be applied to store such optical waveforms by encoding each part of the laser spectrum into specific rotational components.

Besides applicability as storage medium, the use of molecules as light-matter interface for OAM beams features interesting prospects since molecules have an array of attributes which might be well-suited to specific applications. The major role played by molecular alignment on various physical process such as ionization, dissociation, harmonic generation, or laser filamentation could be very valuable especially in the context of optical OAM processing. For instance, the q-plate of aligned molecules reported here can be exploited to transfer the OAM stored in the molecular sample to a harmonic field [51,52] produced by upconversion process. The advantage of the method relies in the production of a pure OAM harmonic light with no need of further polarization selection. In the same purpose, it would also be interesting to investigate how an OAM can be converted from molecules to light when producing a broadband continuum through laser filamentation. The temporal dynamics of molecular alignment could also be attractive by itself. We have shown in this work that the restored OAM for aligned and delocalized molecules is rotated by π due to the fact that the molecular q-plate is rotated between the two configurations. The switch between the two occurs in few hundred of femtosecond and by combining the present approach with unidirectional rotational motion, [30,31] one could produce a molecular q-plate in ultrafast rotation during the revival. The interaction of a pulse with such a dynamically evolving medium would embed a helical phase structure in ultrafast rotation during the pulse resulting for instance in large rotational Doppler shifts. The strategies developed for controlling the molecular dynamics such as pulse shaping [38,39,53] or polarization shaping [30,31] could also be relevant for an extended manipulation of OAM. The optimization of alignment [38,39] or permanent planar delocalization [54] can first be applied in order to improve the degree of molecular alignment and the efficiency of the molecular q-plate. More than that, the possibility of controlling the angular distribution of molecules in space, and through it, the corresponding molecular q-plate is of great interest for the manipulation of OAM and their tunability. As an example, the storage of different OAM states in distinct molecular systems or rotational levels through a judicious shaping [53] would allow to coherently add or subtract OAM fields directly through the molecular interface. In this case, the addition or subtraction would depend on whether the two sets are aligned or anti-aligned.

Another field of interest relies on the phase-matching of the nonlinear process under consideration and the propagation effects of OAM beams. The interaction involving a long range molecular sample, as investigated here, implies very specific phase matching conditions [see Section 4, Supporting information] that can be exploited for useful ap-

plications. We have identified for instance the possibility to design an OAM selector enabling to detect the presence of a given OAM state within an OAM superposition. This can be achieved through a specific coupling scheme for which only the targeted OAM state will be phase-matched so as to provide a significant signal. This will be the subject of one of our future works.

Acknowledgements. The authors sincerely acknowledge Pr. D. Sugny for fruitful discussions and support in the derivation of the Hamiltonian. This work benefited from the facilities of the SMARTLIGHT platform funded by the Agence Nationale de la Recherche (EQUIPEX+ contract "ANR-21-ESRE-0040") and Région Bourgogne Franche-Comté. This work has been supported by the EIPHI Graduate School (contract ANR-17-EURE-0002), Bourgogne-Franche-Comté Region, the CNRS, and the SATT Grand-Est.

Key words: orbital angular momentum, ultrashort optical vortex, field-free molecular alignment

References

[1] L. Allen, M. W. Beijersbergen, R. J. C. Spreeuw, J. P. Woerdman, *Phys. Rev. A* **1992**, *45*, 8185.
[2] M. J. Padgett, *Opt. Express* **2017**, *25*, 11265.
[3] Y. Shen, X. Wang, Z. Xie, C. Min, X. Fu, Q. Liu, M. Gong, X. Yuan, *Light Sci. Appl.* **2019**, *8*, 90.
[4] Y. Yan, G. Xie, M. P. J. Lavery, H. Huang, N. Ahmed, C. Bao, Y. Ren, Y. Cao, L. Li, Z. Zhao, A. F. Molisch, M. Tur, M. J. Padgett, A. E. Willner, *Nat. Commun.* **2014**, *5*, 4876.
[5] J. Wang, J. Y. Yang, I. M. Fazal, N. Ahmed, Y. Yan, H. Huang, Y. Ren, Y. Yue, S. Dolinar, M. Tur, A. E. Willner, *Nat. Photonics* **2012**, *6*, 488.
[6] P. Béjot, B. Kibler, *ACS Photonics* **2021**, *8*, 2345.
[7] P. Béjot, B. Kibler, *ACS Photonics* **2022**, *9*, 2066.
[8] H. He, M. E. J. Friese, N. R. Heckenberg, H. Rubinsztein-Dunlop, *Phys. Rev. Lett.* **1995**, *75*, 826.
[9] N. B. Simpson, K. Dholakia, L. Allen, M. J. Padgett, *Opt. Lett.* **1997**, *22*, 52.
[10] J. Courtial, D. A. Robertson, K. Dholakia, L. Allen, M. J. Padgett, *Phys. Rev. Lett.* **1998**, *81*, 4828.
[11] K. Dholakia, N. B. Simpson, M. J. Padgett, L. Allen, *Phys. Rev. A* **1996**, *54*, 3742
[12] D. Gauthier, P. R. Ribi, G. Adhikary, A. Camper, C. Chappuis, R. Cucini, L. F. DiMauro, G. Dovillaire, F. Frassetto, R. Géneaux, P. Miotti, L. Poletto, B. Ressel, C. Spezzani, M. Stupar, T. Ruchon, G. De Ninno, *Nat. Commun.* **2017**, *8*, 14971.
[13] F. Kong, C. Zhang, F. Bouchard, Z. Li, G. G. Brown, D. H. Ko, T. J. Hammond, L. Arissian, R. W. Boyd, E. Karimi, P. B. Corkum, Nat. Commun. **2017**, *8*, 14970.
[14] F. Kong, C. Zhang, H. Larocque, F. Bouchard, Z. Li, M. Taucer, G. Brown, S. Severino, T. J. Hammond, E. Karimi, P. B. Corkum, *Phys. Rev. Research* **2019**, *1*, 032008.
[15] C. T. Schmiegelow, J. Schulz, H. Kaufmann, T. Ruster, U. G. Poschinger, F. Schmidt-Kaler, *Nat. Commun.* **2016**, *7*, 12998.
[16] K. A. Forbes, D. L. Andrews, *J. Phys. Photonics* **2021**, *3*, 022007.
[17] A. Sit, F. Bouchard, R. Fickler, J. Gagnon-Bischoff, H. Larocque, K. Heshami, D. Elser, C. Peuntinger, K. Günthner, B. Heim, C. Marquardt, G. Leuchs, R. W. Boyd, E. Karimi, *Optica* **2017**, *4*, 1006.
[18] J. Pinnell, I. Nape, M. de Oliveira, N. TabeBordbar, A. Forbes, *Laser Photon Rev.* **2020**, *14*, 2000012.
[19] R. Inoue, N. Kanai, T. Yonehara, Y. Miyamoto, M. Koashi, M. Kozuma, *Phys. Rev. A* **2006**, *74*, 053809.
[20] D. S. Ding, Z. Y. Zhou, B. S. Shi, G. C. Guo, *Nat. Commun.* **2013**, *4*, 2527.
[21] A. Nicolas, L. Veissier, L. Giner, E. Giacobino, D. Maxein, J. Laurat, *Nat. Photonics* **2014**, *8*, 234.
[22] H. Stapelfeldt, T. Seideman, *Rev. Mod. Phys.* **2003**, *75*, 543.
[23] C. P. Koch, M. Lemeshko, D. Sugny, *Rev. Mod. Phys.* **2019**, *91*, 035005.
[24] S. Fleischer, Y. Khodorkovsky, E. Gershnabel, Y. Prior, I. S. Averbukh, *Isr. J. Chem.* **2012**, *52*, 414.
[25] K. Lin, I. Tutunnikov, J. Ma, J. Qiang, L. Zhou, O. Faucher, Y. Prior, I. S. Averbukh, J. Wu, *Advanced Photonics* **2020**, *2*, 024002.
[26] F. Rosca-Pruna, M. J. J. Vrakking, *Phys. Rev. Lett.* **2001**, *87*, 153902.
[27] V. Renard, M. Renard, S. Guérin, Y. T. Pashayan, B. Lavorel, O. Faucher, H. R. Jauslin, *Phys. Rev. Lett.* **2003**, *90*, 153601.
[28] I. V. Litvinyuk, K. F. Lee, P. W. Dooley, D. M. Rayner, D. M. Villeneuve, P. B. Corkum, *Phys. Rev. Lett.* **2003**, *90*, 233003.
[29] J. Itatani, D. Zeidler, J. Levesque, M. Spanner, D. M. Villeneuve, P. B. Corkum, *Phys. Rev. Lett.* **2005**, *94*, 123902.
[30] O. Korech, U. Steinitz, R. Gordon, I. Sh. Averbukh, Y. Prior, *Nat. Photonics* **2013**, *7*, 711.
[31] G. Karras, M. Ndong, E. Hertz, D. Sugny, F. Billard, B. Lavorel, O. Faucher, *Phys. Rev. Lett.* **2015**, *114*, 103001.
[32] J. Ma, H. Zhang, B. Lavorel, F. Billard, E. Hertz, J. Wu, C. Boulet, J. M. Hartmann, O. Faucher, *Nat. Commun.* **2019**, *10*, 5780.
[33] F. Calegari, C. Vozzi, S. Gasilov, E. Benedetti, G. Sansone, M. Nisoli, S. De Silvestri, S. Stagira, *Phys. Rev. Lett.* **2008**, *100*, 123006.
[34] N. Berti, P. Béjot, J. P. Wolf, O. Faucher, *Phys. Rev. A* **2014**, *90*, 053851.
[35] J. Wu, P. Lu, J. Liu, H. Li, H. Pan, H. Zeng, *Appl. Phys. Lett.* **2010**, *97*, 161106.
[36] E. Hertz, B. Lavorel, O. Faucher, *Nat. Photonics* **2011**, *5*, 78.
[37] J. Bert, E. Prost, I. Tutunnikov, P. Béjot, E. Hertz, F. Billard, B. Lavorel, U. Steinitz, I. S. Averbukh, O. Faucher, *Laser & Photon. Rev.* **2020**, *14*, 1900344. .
[38] E. Hertz, A. Rouzée, S. Guérin, B. Lavorel, O. Faucher, Phys. Rev. A **75**(3), 031403 (2007).
[39] A. Rouzée, E. Hertz, B. Lavorel, O. Faucher, *J. Phys. B* **2008**, *41*, 074002.
[40] K. Y. Bliokh, E. A. Ostrovskaya, M. A. Alonso, O. G. Rodríguez-Herrera, D. Lara, C. Dainty, *Opt. Express* **2011**, *27*, 26132.
[41] A. Rubano, F. Cardano, B. Piccirillo, L. Marrucci, *J. Opt. Soc. Am. B* **2019**, *36*, 70.
[42] F. Cardano, E. Karimi, S. Slussarenko, L. Marrucci, C. de Lisio, E. Santamato, *Appl. Opt.* **2012**, *51*, 1.

[43] M. Morgen, W. Price, P. Ludowise, Y. Chen, *J. Chem. Phys.* **1995**, *102*, 8780.
[44] T. Vieillard, F. Chaussard, F. Billard, D. Sugny, O. Faucher, S. Ivanov, J. M. Hartmann, C. Boulet, B. Lavorel, *Phys. Rev. A* **2013**, *87*, 023409.
[45] A. A. Milner, A. Korobenko, V. Milner, *Phys. Rev. A* **2016**, *93*, 053408.
[46] K. Heshami, D. G. England, P. C. Humphreys, P. J. Bustard, V. M. Acosta, J. Nunn, B. J. Sussman, *J. Mod. Opt.* **2016**, *63*, 2005.
[47] B. Kraus, W. Tittel, N. Gisin, M. Nilsson, S. Kröll, J. I. Cirac, *Phys. Rev. A* **2006**, *73*, 020302.
[48] M. Afzelius, C. Simon, H. de Riedmatten, N. Gisin, *Phys. Rev. A* **2009**, *79*, 052329.
[49] J. M. Hartmann, C. Boulet, *J. Chem. Phys.* **2012**, *136*, 184302.
[50] D. Cruz-Delgado, S. Yerolatsitis, N. K. Fontaine, D. N. Christodoulides, R. Amezcua-Correa, M. A. Bandres, *Nat. Photonics* **2022**, 1-6.
[51] J. Houzet, E. Hertz, F. Billard, B. Lavorel, O. Faucher, *Phys. Rev. A* **2013**, *88*, 023859.
[52] E. Skantzakis, S. Chatziathanasiou, P. A. Carpeggiani, G. Sansone, A. Nayak, D. Gray, P. Tzallas, D. Charalambidis, E. Hertz, O. Faucher, *Sci. Rep.* **2016**, *6*, 39295.
[53] M. Renard, E. Hertz, B. Lavorel, O. Faucher, *Phys. Rev. A* **2004**, *69*, 043401.
[54] M. Z. Hoque, M. Lapert, E. Hertz, F. Billard, D. Sugny, B. Lavorel, O. Faucher, *Phys. Rev. A* **2011**, *84*, 013409.